Contrib Mineral Petrol (2013) 166:193–209
DOI 10.1007/s00410-013-0871-8

ORIGINAL PAPER

Chalcophile element geochemistry of the Baima layered intrusion, Emeishan Large Igneous Province, SW China: implications for sulfur saturation history and genetic relationship with high-Ti basalts

Xiao-Qi Zhang · Xie-Yan Song · Lie-Meng Chen · Song-Yue Yu · Wei Xie · Yufeng Deng · Jia-Fei Zhang · Shu-Guang Gui

Received: 23 October 2012 / Accepted: 5 March 2013 / Published online: 27 March 2013

Abstract The Permian Baima mafic layered intrusion, believed to be related to the S-undersaturated Emeishan high-Ti basalts, hosts a giant Fe–Ti-V oxide deposit in the lower part of the intrusion. Uniformly high Cu/Pd (1.9×10^6–6.1×10^4) and low Pd/Zr (<0.1) indicate that the Baima parental magma experienced prior sulfide segregation. Mantle-liked $\delta^{34}S$ values and low S/Se values indicate negligible external sulfur addition. Primitive mantle-normalized PGE patterns and MELTS calculations indicate that extensive fractional crystallization (~59 %) of chromite, olivine and pyroxene at depth drove the primitive picritic magma to S saturation. Strong positive correlation between IPGE and PPGE and between PGE and V, Cr and S suggest that magmatic sulfide is the dominant mineral controlling the distribution of PGE in the Baima intrusion. A positive correlation between S and Cr, $FeO_T + TiO_2$ and V content, together with MELTS calculations, indicate that the parental magma of the Baima intrusion reached a second stage of S saturation in the shallower Baima magma chamber, which was likely triggered by decreasing Fe^{2+} accompanying magnetite precipitation. Primitive mantle-normalized PGE patterns for Baima intrusion rocks display similar trends to high-Ti basalts inside the Panxi area, suggesting that they are co-magmatic, and following a similar differentiation trend. However, the lavas erupted before they reached sulfide saturation. The more evolved nature of high-Ti basalts outside the Panxi area indicate that they experienced more extensive pre-eruption fractional crystallization. Further fractional crystallization process led these lavas show more PGE fractionated feature.

Keywords Emeishan large igneous province · Panxi area · Layered intrusion · High-Ti basalts · Chalcophile elements · Sulfide saturation

Introduction

Large layered intrusions commonly host reef-type platinum-group element (PGE) mineralization, including the Merensky Reef, UG1 and UG2 Reefs in the Bushveld Complex and the J-M Reef in the Stillwater Complex (Campbell et al. 1983; McCallum 1996; Naldrett 2004; Wilson and Chunnett 2006). The PGE reefs are hosted by pyroxenitic to noritic cumulates or chromitite layers in the lower parts of the intrusions. Magnetite-bearing layers in the upper zones of these layered intrusions are generally barren of economic PGE mineralization, because by the time magnetite crystallized PGE had already been removed from the magma onto early formed sulfides and platinum-group minerals (Sá et al. 2005). However, recent studies have shown that a basaltic magma may become saturated in Fe–Ti oxides and a sulfide liquid at approximately the same time (Andersen et al. 1998; Andersen 2006; Prendergast 2000; Maier et al. 2003; Barnes et al. 2004; Sá et al. 2005).

Communicated by J. Hoefs.

X.-Q. Zhang · X.-Y. Song (✉) · L.-M. Chen · S.-Y. Yu · W. Xie · Y. Deng
State Key Laboratory of Ore Deposit Geochemistry, Institute of Geochemistry, Chinese Academy of Sciences, 46th Guanshui Road, Guiyang 550002, China
e-mail: songxieyan@vip.gyig.ac.cn

X.-Q. Zhang
Graduate University of the Chinese Academy of Sciences, Beijing 100049, China

J.-F. Zhang · S.-G. Gui
Panzhihua Group Company Ltd., Panzhihua, Sichuan, China

Thus, prospective PGE mineralization can be also associated with the magnetite-rich layers, especially in the tholeiitic magma which remained uncontaminated during ascent and crystallization (Maier et al. 2003).

The Baima layered intrusion is one of the largest layered intrusions in the Emeishan Large Igneous Province (ELIP) of SW China. Previous geochronological and Sr–Nd isotope data demonstrated that the Baima Fe–Ti oxide-bearing layered intrusion is likely to be broadly comagmatic with the Emeishan high-Ti basalts, which are thought to be derived via relatively high degree of partial melting (15–20 %) of the Emeishan mantle plume with only weak crustal contamination (Xiao et al. 2004; Zhou et al. 2008; Qi and Zhou 2008; Song et al. 2005, 2008a, b, 2009; Shellnutt et al. 2009; Pang et al. 2010; Zhong et al. 2011a). Based on mineral compositions and MELTS modeling, our study has indicated that the magnetite layers in the lower part of the Baima intrusion formed by early crystallization of Fe–Ti oxides from frequent replenished, evolved Fe–Ti–rich magmas (~61 % fractional crystallization) ascending from deeper levels in the crust or upper mantle (Zhang et al. 2012).

Although Baima has been the focus of significant previous research, none has addressed its sulfide saturation history and PGE fractionation processes. Study of the PGE will also better constrain the proposed genetic relationship

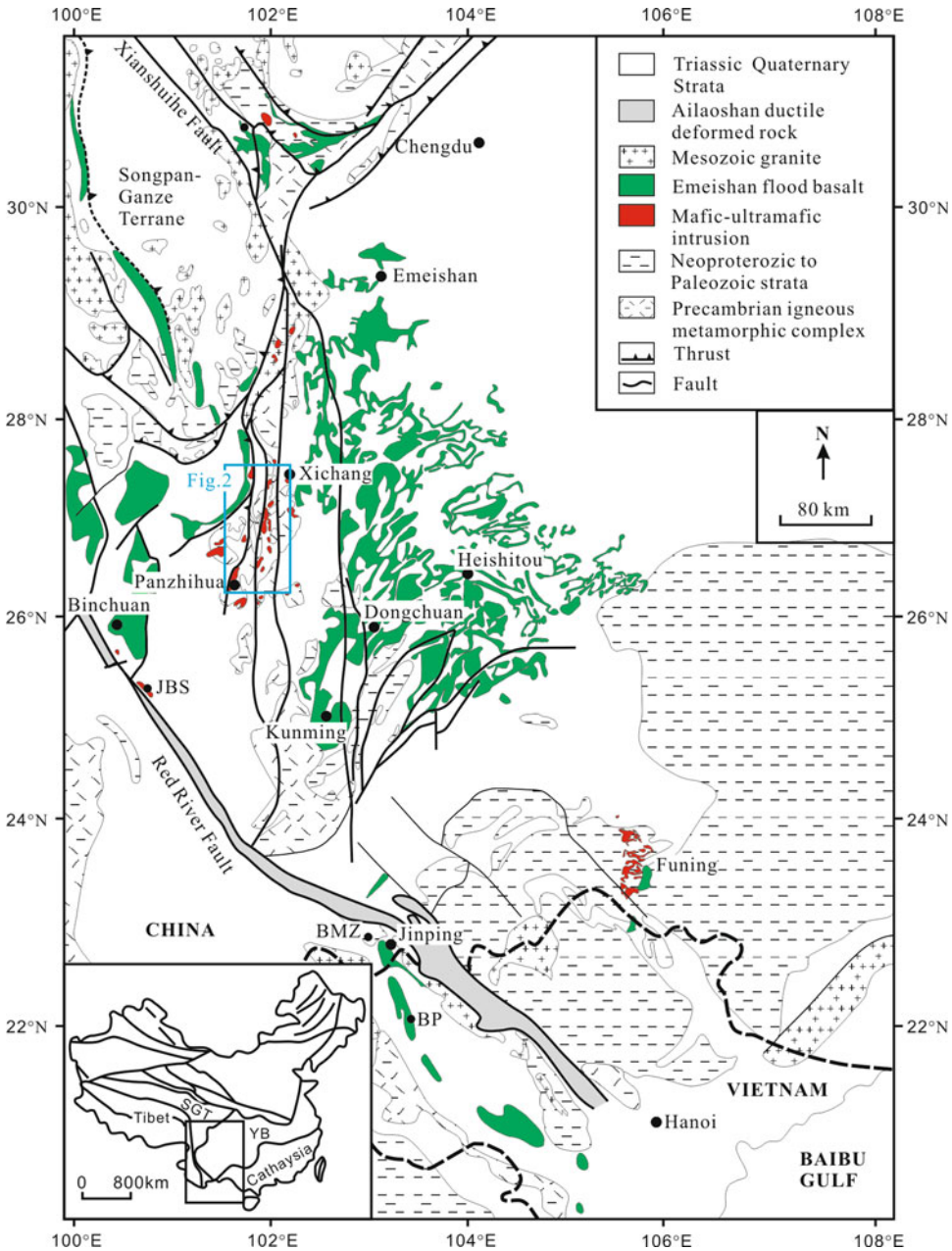

Fig. 1 Geological map of the Emeishan Large igneous province, SW China (Modified after Song et al. 2009)

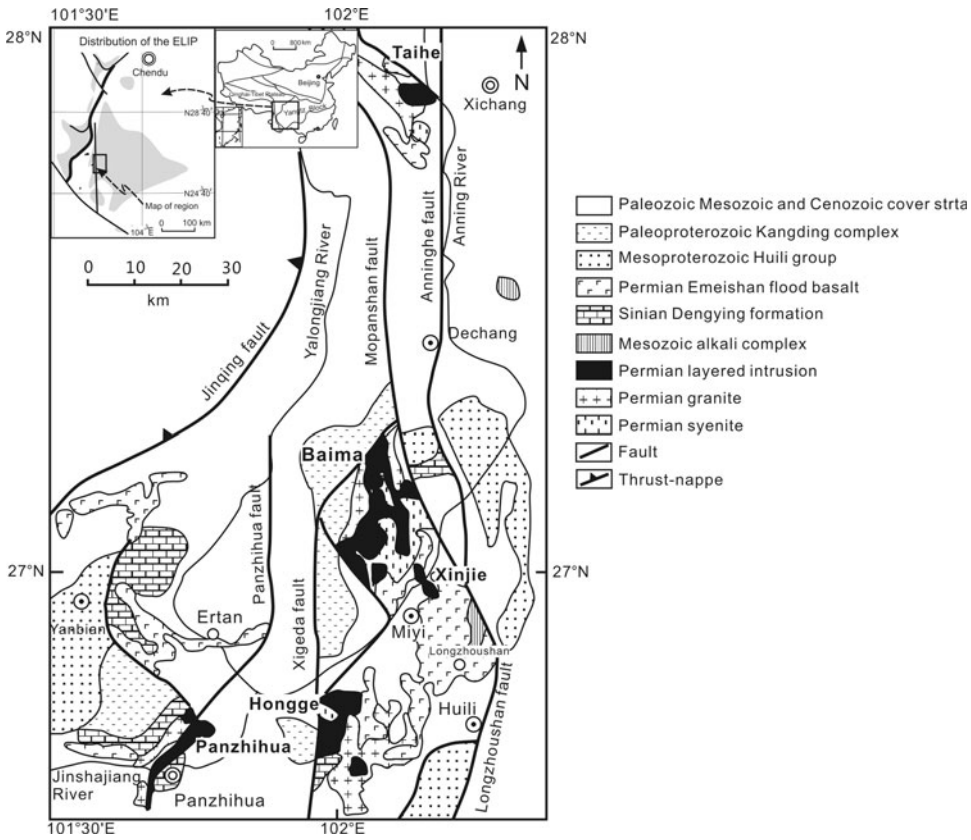

Fig. 2 Regional geological map of the Pan-Xi (Panzhihua-Xichang) area, showing the distribution of layered mafic–ultramafic intrusions (modified after Zhong et al. 2005)

between the Baima intrusion and the high-Ti basalts. Hence, this study uses the chalcophile and selected trace element data to address several outstanding questions, such as the following: (1) the sulfide saturation history in the Baima layered intrusion; (2) the major trigger for sulfide saturation and (3) the relationship between the Baima intrusion and the high-Ti basalts. Our study reveals that the parental magma of the Baima layered intrusion experienced two stages of sulfide saturation. Extensive fractional crystallization ($\sim$ 59 %) and early magnetite precipitation are the key factors controlling sulfide segregation in the deep and shallow magma chamber, respectively. The Baima intrusion

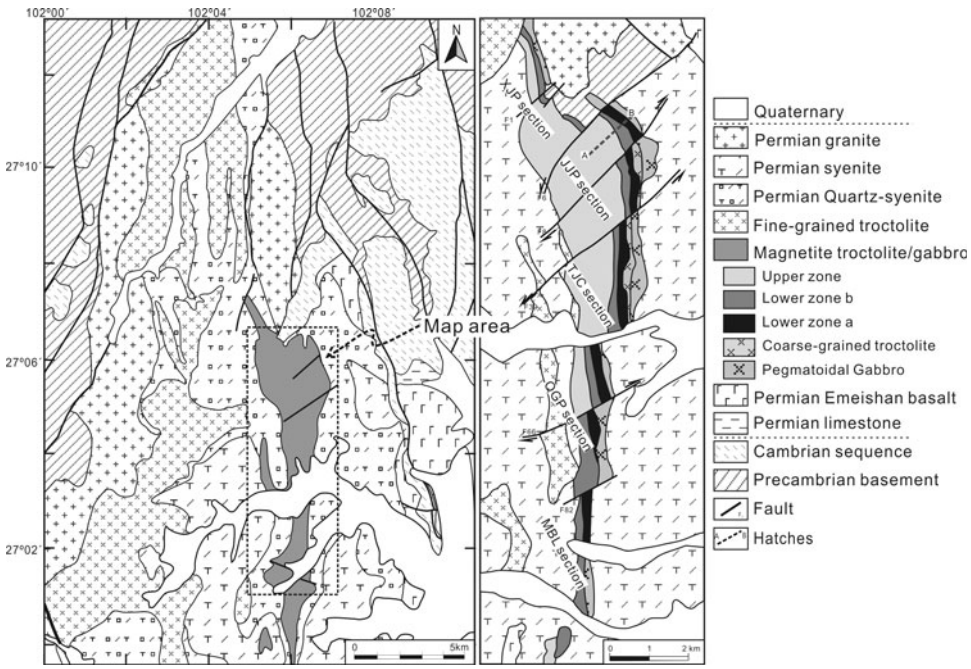

Fig. 3 Simplified regional geological map of the Baima layered intrusion (modified after PXGU, 1984). Section name: XJP (Xiajiaping), JJP (Jijiping), TJC (Tianjiacun), QGP (Qinggangping), MBL (Mabinlang)

and the high-Ti basalts are originally comagmatic, but the latter erupted before the magma reached sulfide saturation.

Geological background

The ~ 260 Ma Emeishan Large Igneous Province (ELIP) covers an area more than 5×10^5 km^2 in southwestern China and northern Vietnam, and has been inferred to have been derived from a Late Permian mantle plume (Fig. 1) (Chung and Jahn 1995; Xu et al. 2001; Song et al. 2001, 2004; He et al. 2003, 2007; Xiao et al. 2004 and references there in). It consists of the Emeishan continental flood basalts, associated mafic–ultramafic intrusions and related felsic intrusions. The Emeishan basalts have been divided into low-Ti (Ti/Y < 500) and high-Ti (Ti/Y > 500) groups (Xu et al. 2001; Xiao et al. 2004). The low-Ti basalts are mainly distributed in the central part of the ELIP and are usually linked with Ni-Cu-PGE-bearing mafic-ultramafic intrusions, whereas the high-Ti basalts are distributed both in the central and outer zone of the ELIP are considered to be broadly comagmatic with the Fe–Ti-V-bearing layered intrusions (Xu et al. 2001; Xiao et al. 2004; Song et al. 2005, 2008a, b; Zhou et al. 2008; Chen et al. 2010). In addition, the high-Ti basalts are commonly PGE-undepleted and experienced fractionation of olivine, chromite, pyroxenes, plagioclase and PGE-minerals under S-undersaturated condition (Xu et al. 2001; Xiao et al. 2004; Qi et al. 2008; Qi and Zhou 2008; Song et al. 2009; Wang et al. 2011).

The Panxi (Panzhihua-Xichang) area is located in the central part of the ELIP where several mafic–ultramafic layered intrusions host the most economically important Fe–Ti oxide deposits in China (Figs. 1, 2). These layered intrusions are distributed in an N–S trending zone and include from north to south: the Taihe (undated), Baima (262 ± 2 Ma), Xinjie (259 ± 3 Ma), Hongge (259 ± 1.3 Ma) and Panzhihua (263 ± 3 Ma) intrusions (Zhou et al. 2002, 2005, 2008; Zhong and Zhu 2006). They comprise predominantly gabbro, olivine gabbro and troctolite (Taihe, Baima, Panzhihua) or peridotite, olivine clinopyroxenite, clinopyroxenite and gabbro (Hongge and Xinjie) (Fig. 2) (PXGU 1984; Zhong et al. 2002, 2004; Pang et al. 2008; Zhou et al. 2005). Some of the layered intrusions, such as Baima, Panzhihua and Hongge, were emplaced into Late Neoproterozoic metamorphic rocks, whereas the Xinjie intrusion was intruded into the Emeishan flood basalts (PXGU 1984, Zhong et al. 2003, 2004, 2011b; Bai et al. 2012b; Zhou et al. 2008).

Geology and petrography of the Baima intrusion

The N–S striking Baima mafic layered intrusion is ~ 24 km long and 2–6.5 km wide and dips 50–70° west. The intrusion is emplaced into Sinian metamorphic sandstone, phyllite, slate and marble (Fig. 3). After emplacement, the Baima intrusion was surrounded and cut by ~ 259 Ma syenitic intrusions and dykes (PXGU 1984). In addition, several NW–SE-trending faults subdivide the Baima intrusion into five segments, including Xiajiaping, Jijiping, Tianjiacun, Qinggangping and Mabinglang (Fig. 3). Along strike, the Baima intrusion shows a thickness gradation from north to south.

Based on textures and mineral assemblages, the Baima layered intrusion is divided into a Fe–Ti-V oxide-mineralized lower zone (LZ) and an apatite-bearing upper zone (UZ). The boundaries between the LZ and the UZ have been defined by a sharp increase in plagioclase and the appearance of apatite (Zhang et al. 2012). The LZ is further subdivided into LZa and LZb, based on olivine/clinopyroxene ratio and textures. The LZa is ~120 m thick and dominated by thick medium-grained magnetite troctolite, interlayered with thin layer of troctolite (with <5 modal % Fe–Ti oxide). LZb is nearly 200 m thick and mainly consists of magnetite troctolite with interlayer of troctolite and olivine gabbro. The magnetite troctolite typically contains 20–55 modal % titanomagnetite, 2–10 modal % ilmenite, 25–40 % olivine, <20 % plagioclase and <15 % clinopyroxene. The troctolite consists of 20–30 % olivine, 35–55 % plagioclase, <15 % clinopyroxene and <20 % Fe–Ti oxides. The olivine gabbro differs from the troctolite in having a higher

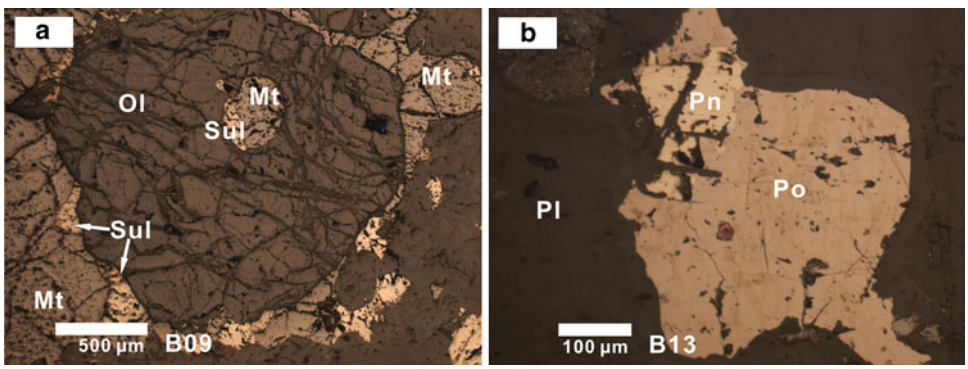

Fig. 4 Photomicrographs of sulfide minerals of the Baima intrusion (reflected light). **a** interstitial sulfides between magnetite and silicate minerals **b** interstitial pyrrhotite with pentlandite exsolutions. *Ol* olivine, *Pl* plagioclase, *Mt* magnetite, *Sul* sulfide, *Po* pyrrhotite, *Pn* pentlandite

Table 1 Platinium-group elements, Ni, Cu and Zr concentrations of the Baima layered intrusion (The LLD for Se is >0.5 ppm)

Section	Zone	Sample	Rock	Ni (ppm)	Ir (ppb)	Ru (ppb)	Rh (ppb)	Pt (ppb)	Pd (ppb)	Cu (ppm)	S (wt %)
Jijiping section	Upper zone (UZ)	B39	Mt- Troctolite	63.4	0.01	0.01	0.01	0.22	0.25	75.6	0.32
		B38	Troctolite	32.3						29.3	0.08
		B37	Troctolite	45.1	0.01	0.01	0.01	0.09	0.22	51.8	0.18
		B32	Gabbro	51.3						72.5	0.21
		B31	Gabbro	43.6	0.01	0.01	0.01	0.10	0.11	48.4	0.15
		B30	Troctolite	69.8	0.01	0.01	0.01	0.18	0.19	78.5	0.26
		B29	Gabbro	48.4	0.01	0.01	0.01	0.09	0.09	64.2	0.23
		B28	Ol- Gabbro	40.8	0.00	0.01	0.00	0.09	0.07	48.2	0.16
	Lower zone b (LZb)	B27	Mt- Troctolite	166						238	0.72
		B25	Mt- Troctolite	175	0.02	0.02	0.01	0.48	0.36	189	0.47
		B24	Troctolite	103	0.01	0.01	0.01	0.25	0.19	131	0.4
		B21	Mt- Troctolite	166						204	0.61
		B20	Gabbro	80.6	0.03	0.05	0.02	0.22	0.19	89.6	0.23
		B19	Mt- Troctolite	161	0.01	0.02	0.01	0.18	0.21	185	0.46
	Lower zone a (LZa)	B18	Mt- Troctolite	226	0.01	0.14	0.08	0.29	1.1	251	0.62
		B17	Mt- Troctolite	192						158	0.30
		B16	Mt- Troctolite	432	0.58	0.64	0.80	19.8	19.6	578	0.72
		B15	Mt- Troctolite	256	0.02	0.04	0.02	0.42	0.36	307	0.52
		B14	Mt- Troctolite	372	1.4	1.5	1.4	34.2	17.6	306	0.41
		B13	Mt- Troctolite	284	0.04	0.03	0.03	0.69	0.74	425	1.0
		B11	Mt- Troctolite	441	0.31	0.49	0.23	5.8	6.8	358	0.30
		B10	Troctolite	224	0.06	0.05	0.08	3.0	1.8	111	0.09
		B09	Mt- Troctolite	307	0.03	0.03	0.02	0.49	0.36	383	1.1
		B08	Mt- Troctolite	382	0.02	0.03	0.02	0.41	0.40	544	1.1
Qing gangping section	Lower Zone b (LZb)	Q14	Ol- Gabbro	32.7	0.00	0.00	0.00	0.07	0.16	45.2	0.23
		Q13	Gabbro	20.1	0.00	0.00	0.00	0.07	0.08	38.6	0.22
		Q12	Troctolite	43.4						75.1	0.35
		Q11	Gabbro	13.1	0.00	0.00	0.00	0.02	0.06	32.1	0.16
		Q10	Gabbro	32.3	0.00	0.00	0.00	0.07	0.19	46.1	0.26
		Q09	Gabbro	51.2						56.0	0.32
		Q07	Mt- Troctolite	65.5	0.01	0.01	0.01	0.39	0.35	97.3	0.59
		Q06	Gabbro	55.8	0.00	0.00	0.00	0.12	0.15	40.6	0.34
		Q05	Ol- Gabbro	53.8	0.03	0.03	0.03	0.98	0.66	43.9	0.34
		Q04	Mt- Troctolite	295	0.01	0.01	0.01	0.23	0.25	474	0.9
		Q03	Troctolite	58.8						56.8	0.43
		Q02	Mt- Troctolite	233	0.01	0.03	0.01	0.13	0.20	371	0.71
		Q01	Mt- Troctolite	254	0.01	0.01	0.01	0.25	0.38	384	0.64

Table 1 continued

Section	Zone	Sample	Rock	Se (ppm)	Zr (ppm)	Σ PGE (ppm)	Cu/Pd	Pt/Pd	Cu/Zr	Pd/Zr	S/Se
Jijiping section	Upper zone (UZ)	B39	Mt- Troctolite	2.0	16.9	0.49	3.1×10^5	0.89	4.47	0.01	1,600
		B38	Troctolite	1.0	13.9				2.11		800
		B37	Troctolite	1.3	16.2	0.33	2.4×10^5	0.42	3.2	0.01	1,385
		B32	Gabbro	1.5	16.4				4.42		1,400
		B31	Gabbro	1.1	23.2	0.23	4.6×10^5	0.91	2.09	0.00	1,364
		B30	Troctolite	1.3	12.2	0.40	4.2×10^5	0.96	6.43	0.02	2,000
		B29	Gabbro	1.3	11.6	0.20	6.8×10^5	0.95	5.53	0.01	1,769
		B28	Ol- Gabbro	1.2	13.1	0.19	6.5×10^5	1.23	3.68	0.01	1,333
	Lower zone b (LZb)	B27	Mt- Troctolite	3.4	21.5				11.1		2,118
		B25	Mt- Troctolite	3.3	8.9	0.89	5.3×10^5	1.34	21.2	0.04	1,424
		B24	Troctolite	2.3	11.4	0.47	7.0×10^5	1.31	11.5	0.02	1,739
		B21	Mt- Troctolite	3.6	12.3				16.6		1,694
		B20	Gabbro	1.5	15.3	0.51	4.7×10^5	1.16	5.85	0.01	1,533
		B19	Mt- Troctolite	3.0	14.1	0.43	8.8×10^5	0.84	13.1	0.01	1,533
	Lower zone a (LZa)	B18	Mt- Troctolite	3.8	9.5	1.7	2.2×10^5	0.26	26.5	0.12	1,632
		B17	Mt- Troctolite	3.2	10.8				14.7		938
		B16	Mt- Troctolite	3.3	9.0	41.4	3.0×10^4	1.01	64.5	2.2	2,182
		B15	Mt- Troctolite	4.9	22.7	0.87	8.5×10^5	1.15	13.5	0.02	1,061
		B14	Mt- Troctolite	3.3	11.9	56.1	1.7×10^4	1.94	25.7	1.5	1,242
		B13	Mt- Troctolite	5.1	12.2	1.6	5.7×10^5	0.93	34.9	0.06	1,980
		B11	Mt- Troctolite	4.2	19.9	13.6	5.3×10^4	0.86	18.0	0.34	714
		B10	Troctolite	1.0	30.4	5.1	6.1×10^4	1.68	3.66	0.06	900
		B09	Mt- Troctolite	5.0	18.4	0.9	1.1×10^6	1.34	20.8	0.02	2,224
		B08	Mt- Troctolite	4.9	14.6	0.92	1.4×10^6	1.03	37.2	0.03	2,240
Qing gangping section	Lower Zone b (LZb)	Q14	Ol- Gabbro	2.0	21.6	0.24	2.9×10^5	0.45	2.09	0.01	1,150
		Q13	Gabbro	1.6	20.6	0.17	4.6×10^5	0.86	1.87	0.00	1,375
		Q12	Troctolite	3.3	21.7				3.46		1,061
		Q11	Gabbro	1.2	16.3	0.10	5.0×10^5	0.38	1.97	0.00	1,333
		Q10	Gabbro	1.9	20.5	0.27	2.5×10^5	0.39	2.25	0.01	1,368
		Q09	Gabbro	2.4	21.2				2.64		1,333
		Q07	Mt- Troctolite	4.1	23.3	0.78	2.8×10^5	1.12	4.18	0.01	1,439
		Q06	Gabbro	2.1	20.5	0.29	2.6×10^5	0.80	1.98	0.01	1,619
		Q05	Ol- Gabbro	2.0	13.0	1.7	6.6×10^4	1.48	3.38	0.05	1,700
		Q04	Mt- Troctolite	4.6	10.4	0.50	1.9×10^6	0.90	45.6	0.02	1,957
		Q03	Troctolite	2.3	15.1				3.76		1,870
		Q02	Mt- Troctolite	3.7	9.9	0.37	1.8×10^6	0.63	37.7	0.02	1,919
		Q01	Mt- Troctolite	3.9	9.7	0.65	1.0×10^6	0.66	39.5	0.04	1,641

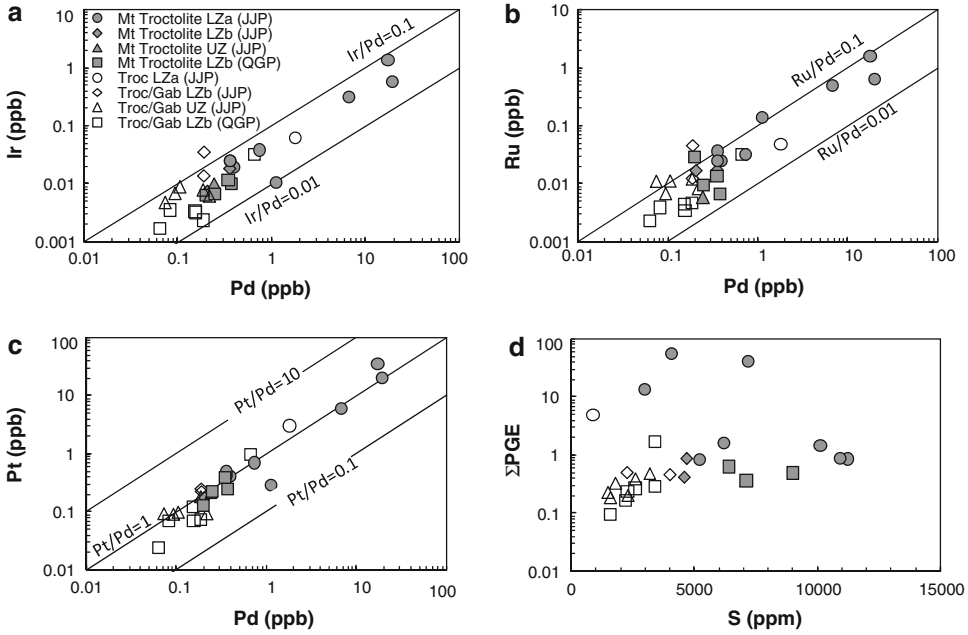

Fig. 5 Bivariant diagrams between Ir, Ru, Pt vs. Pd (**a**, **b**, **c**) and total PGE versus sulfur (**d**). *Troc* troctolite, *Gab* gabbro

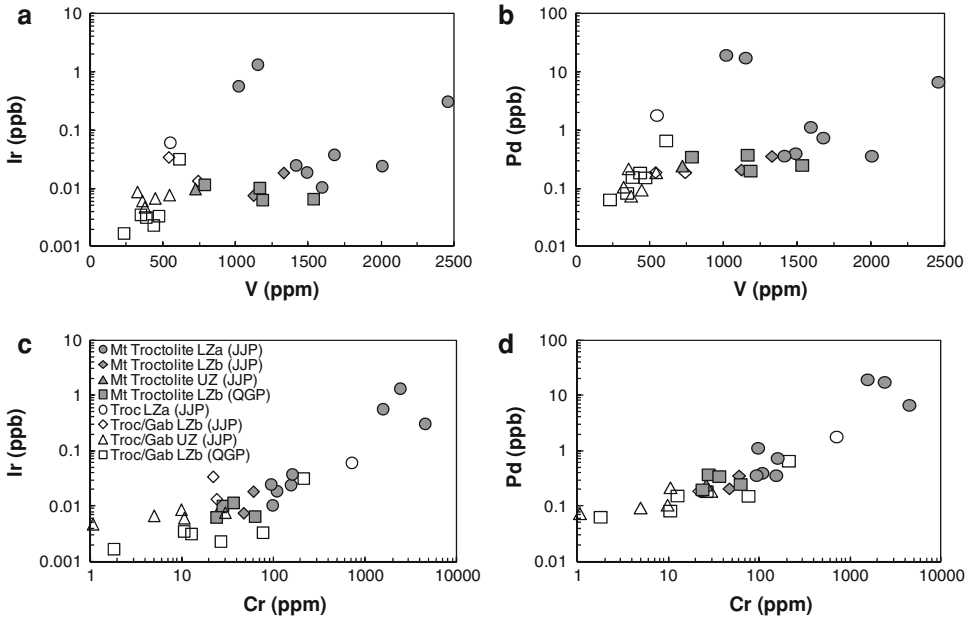

Fig. 6 Binary plots of Ir and Pd with V (**a**, **b**) and Cr (**c**, **d**). *Troc* troctolite, *Gab* gabbro

proportion of clinopyroxene. The UZ, with a thickness of ~1,060 m, mainly consists of troctolite and olivine gabbro and is characterized by having considerably less magnetite (<10 up to 15 %) and abundant plagioclase (>50 %) relative to LZa and LZb. The appearance of apatite (up to 2 %) is also a key feature of the UZ.

Sulfides occur as interstitial accessory minerals and are dominantly pyrrhotite with minor pentlandite exsolutions (Fig. 4). The abundance of magmatic sulfides correlates positively with Fe–Ti oxides. They are most abundant in the magnetite troctolite in the LZ (1 % to 3 %), and are much less abundant (1 %) in the gabbros in the UZ.

Analytical methods and results

Analytical methods

PGE analyses were done by isotope dilution ID-ICP-MS using an improved Carius tube technique (Qi et al. 2007) at the Institute of Geochemistry, Chinese Academy of Sciences. Eight grams of disseminated oxide rock powder and 10 g of troctolite and gabbro powder were digested with 35 ml aqua regia in a 75-ml Carius tube placed in a sealed, custom-made, high-pressure, water-filled autoclave. Ir, Ru, Pt and Pd were measured by isotope dilution, and ^{194}Pt was

Table 2 Blank (ng), detection limits (DL) (ng/g) and analytical results (ng/g) of reference materials, TDB-1, WGB-1 and UMT-1

Elements	Blank	DL	TDB-1 Measured	Qi et al.	Meisel	Certified	WGB-1 Measured	Qi et al.	Meisel	Certified	UMT-1 Measured	Meisel	Certified
Ir	0.001	0.001	0.08	0.08 ± 0.01	0.075	0.15	0.20	0.16 ± 0.02	0.211	0.33	9.1	8.61	8.8
Ru	0.001	0.001	0.27	0.22 ± 0.02	0.198	0.3	0.14	0.13 ± 0.01	0.144	0.3	9.9	10.1	10.9
Rh	0.002	0.001	0.45	0.48 ± 0.03	0.471	0.7	0.19	0.20 ± 0.02	0.234	0.32	10.4	9.1	9.5
Pt	0.002	0.009	4.7	5.23 ± 0.28	5.01	5.8	5.2	6.34 ± 0.61	6.39	6.1	133	146	129
Pd	0.025	0.015	23.5	23.0 ± 1.2	24.3	22.4	12.1	13.0 ± 1.1	13.9	13.9	105	113	106

Referenced data are cited from Qi et al. (2008); *Meisel* (Meisel and Moser 2004); *Certified* (Govindaraju 1994)

Table 3 Sulfur isotope compositions of selected lithology in the Baima layered intrusion (LLD > 0.2 ‰)

Section	Zone	Sample	Rock	$\delta^{34}S_{V\text{-}CDT}$ (‰)
Jijiping section	Upper zone (UZ)	B39	Mt-Troctolite	1.6
		B37	Troctolite	1.4
		B31	Gabbro	1.1
		B30	Troctolite	1.6
		B29	Gabbro	2.2
		B28	Ol-Gabbro	1.5
	Lower zone b (LZb)	B25	Mt-Troctolite	2.7
		B24	Troctolite	2.1
		B20	Gabbro	1.0
		B19	Mt-Troctolite	2.5
	Lower zone a (LZa)	B18	Mt-Troctolite	2.2
		B16	Mt-Troctolite	2.3
		B15	Mt-Troctolite	2.6
		B14	Mt-Troctolite	1.8
		B13	Mt-Troctolite	1.3
		B11	Mt-Troctolite	1.5
		B09	Mt-Troctolite	0.9
		B08	Mt-Troctolite	0.6
Qing gangping section	Lower zone b (LZb)	Q14	Ol-Gabbro	1.9
		Q11	Gabbro	1.7
		Q09	Gabbro	1.3
		Q06	Gabbro	1.9
		Q05	Ol-Gabbro	1.2
		Q04	Mt-Troctolite	1.1
		Q02	Mt-Troctolite	1.8
		Q01	Mt-Troctolite	0.9

used as the internal standard to calculate the abundance of mono-isotopic Rh (Qi et al. 2004). Reference standards TDB-1, WGB-1 and UMT-1 were analyzed to monitor accuracy. Analytical results for total procedural blanks and standard reference materials are listed in Table 2. Results for TDB-1 and WGB-1 agree well with values reported by Qi and Zhou (2008), and the result for UMT-1 is in good agreement with certified values.

Copper, Ni, Zr and V contents were analyzed, using a Perkin-Elmer EIAN DRC-e ICP-MS at the Institute of Geochemistry, Chinese Academy of Sciences, Guiyang. Fifty milligrams of powder was dissolved using the method described by Qi et al. (2000), and 500 mg/ml Rh was used as an internal standard. Standard additions and pure elemental standards were used for external calibration and standards MSAN, OU-6, AMH-1, GBPG-1 as reference materials. Accuracy and precision of the ICP-MS analyses are estimated to be better than 5 % for all analyzed elements. Whole-rock S was determined by the LECO

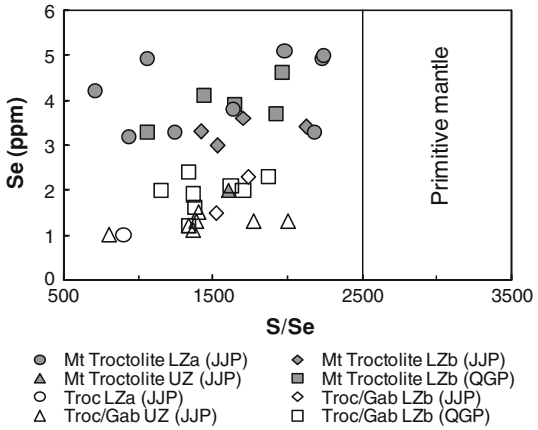

Fig. 7 Binary plots of S/Se and Se. Referenced primitive mantle S/Se ratio (2,500–3,500) is from Lorand et al. (2003). *Troc* troctolite, *Gab* gabbro

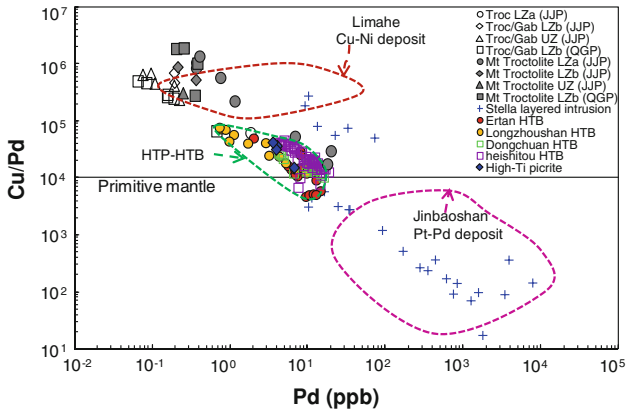

Fig. 8 Plots of Cu/Pd versus Pd in rocks of the Baima intrusion. Reference data are from (Maier et al. 2003; Zhong et al. 2006; Tao et al. 2007, 2008; Qi et al. 2008, Qi and Zhou 2008; Song et al. 2009; Li et al. 2012). *Troc* troctolite, *Gab* gabbro

induction furnace-titration method, and Se was analyzed using ICP-MS at the ALS Chemex Ltd. (Guangzhou). Analytical precision for S was better than ± 0.02 wt %, and for Se was better than ± 0.5 ppm. Sulfur isotopic analysis was conducted using an EA-IRMS (Elemental Analyzer and stable Isotope ratio mass spectrometer) at the Institute of Geochemistry, Chinese Academy of Sciences, Guiyang. Analytical precision was better than ± 0.2 ‰. MgO and TiO_2 data discussed in this study are presented from Zhang et al. (2012). The analyzed trace element and PGE abundances of the samples are given in Table 1 and S isotope data are given in Table 3.

Analytical results

Concentrations of chalcophile elements and selected trace elements of representative rocks from the Baima intrusion are listed in Table 1. Total PGE contents (ΣPGE) of most Baima samples range from 0.19 to 5.1 ppb. Average PGE contents decrease from 1.6 ppb in the LZa to 0.38 ppb in the LZb and 0.23 ppb in the UZ. Three samples in LZa (sample B11, B14 and B16) have much higher ΣPGE contents than in adjacent layers varying from 13.6 to 41.4 ppb (Table 1). Based on whole-rock Cr and plagioclase An content, Zhang et al. (2012) suggested that these three layers represent separate, temporally distinct magma pulses. The PGE have good inter-element correlations (Fig. 5a, b, c) and are also roughly positive correlated with S (Fig. 5d). A few samples from LZa have notably high ΣPGE relative to the other samples at comparable S contents (Fig. 5d). Ir and Pd show roughly positive correlations with whole-rock V and Cr contents (Fig. 6), although a few samples have higher contents of Ir and Pd at the comparable V contents.

Nickel contents of the rocks range from 13 to 441 ppm and Cu from 29 to 578 ppm (Table 1). Average Ni and Cu contents are highest in the LZ and decrease dramatically into the UZ (Table 1). All samples have higher Cu/Pd (1.9×10^6–6.1×10^4) than the primitive mantle; however, the Cu/Pd values are relatively lower in three LZa samples (1.7×10^4–5.3×10^4) (Table 1; Fig. 8). Rocks from the Baima intrusion have lower Pd/Zr (0–0.12, except for three samples) than the primitive mantle (1.18) (Table 1).

Primitive mantle-normalized PGE patterns show trends very similar to those of high-Ti basalts inside the Panxi area, with a flat or slightly decreasing trend from Ni to Ir and Ru, but slightly rising from Ru to Pt and then show a flat trend from Pt to Pd, finally increasing from Pd to Cu (Fig. 9). Both, however, show a moderate PPGE-enrichment trend compared with the high-Ti basalts from outside the Panxi area (Fig. 9; Table 2).

Sulfur contents of the Baima rocks vary from 0.08 to 1.1 wt %, and the $\delta^{34}S$ values show a narrow scatter, ranging from 0.59 to 2.66 ‰ with a mean value of 1.64 ± 0.11 ‰ (1 σn = 26) (Table 3). Except for three magnetite troctolites in the LZa (sample B11, B14 and B16), the S contents of most samples are high in magnetite layers than in troctolite or olivine gabbro (Table 1). Se contents of most samples are >3 ppm in the magnetite troctolite, but <3 ppm in the troctolite. The S/Se values (714–2,240, Table 1) are much lower than the primitive mantle (2,500–3,500, Lorand et al. 2003) (Fig. 7).

Discussions

Sulfide segregation in deep level

The partition coefficients for Ir and Pd between sulfide and silicate melt are nearly two orders of magnitude greater than those of Cu and Ni (e.g. $D_{Ir} = 3.4 \times 10^4$; $D_{Pd} = 3.4 \times 10^4$; $D_{Cu} = 5.8 \times 10^2$; $D_{Ni} = 1.3 \times 10^3$; (Peach

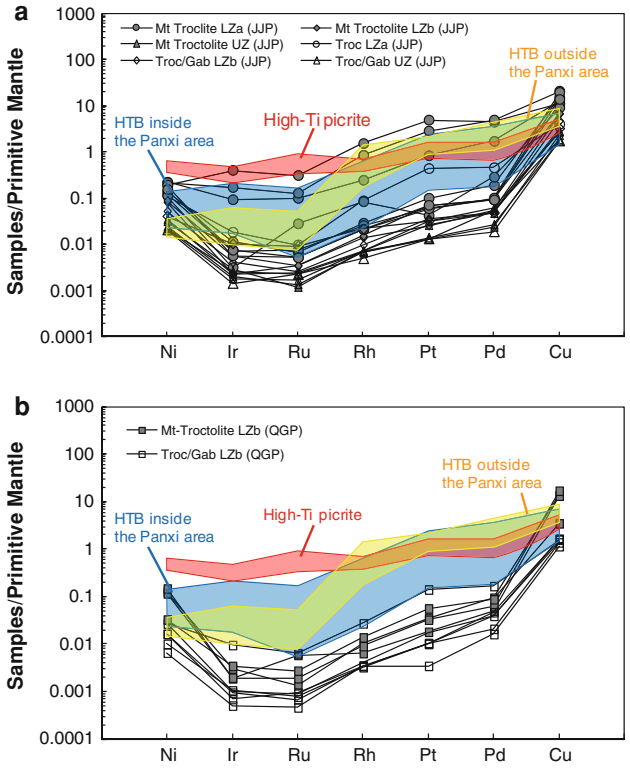

Fig. 9 Primitive mantle-normalized platinum-group element diagrams of two sections of the Baima intrusion. Referenced high-Ti basalt (HTB) data from inside the Panxi area (the Ertan and Longzhzoushan basalts) are from Zhong et al. (2006), Qi et al. (2008), Song et al. (2009); high-Ti basalt (HTB) data from outside the Panxi area (the Dongchuan and Heishitou basalts) are from Qi and Zhou (2008), Song et al. (2009); the referenced high-Ti picrite data are from Li et al. (2012). Normalizing values are from Taylor and McLennan (1985). *Troc* troctolite, *Gab* gabbro

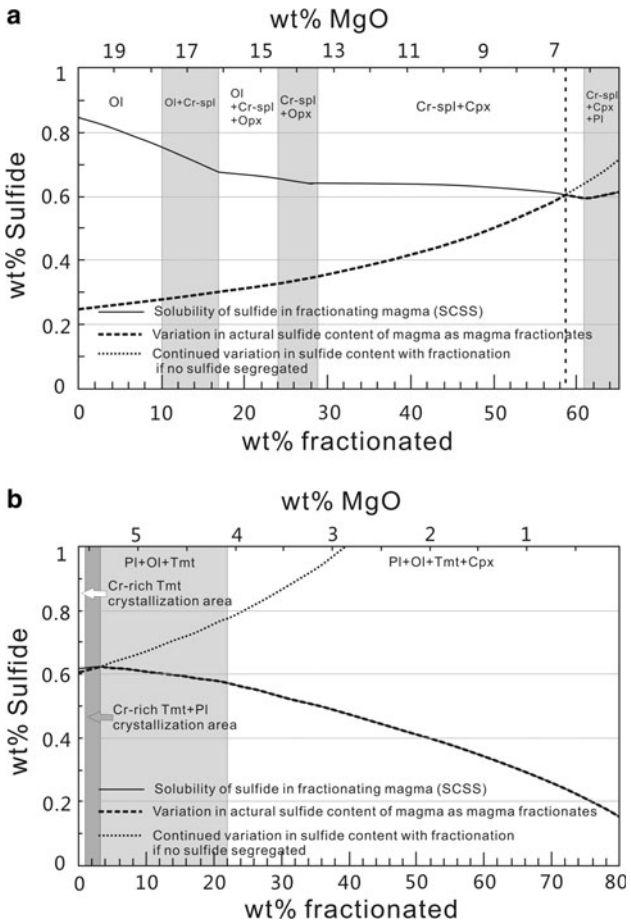

Fig. 10 **a** Variation in SCSS, actual sulfide content of the magma and sulfide content if no sulfide segregation occurred, and assuming 1,000 ppm as initial sulfide content. The MELTS calculation was performed by Zhang et al. (2012) at 5 kbar under a closed to oxygen system. The melt inclusion data in high-Ti picrite olivine phenocryst were taken as the starting composition (Kamenetsky et al. 2012). The SCSS curve is calculated using the equation of Li and Ripley (2009) **b** Variation of SCSS in the Baima intrusion. Assuming the initial sulfide content in the Baima intrusion is equal to the sulfide content at sulfur saturation in the primary magma. The MELTS calculation was performed by Zhang et al. (2012) at 1.5 kbar under a closed to oxygen system. The SCSS curve is calculated using the equation of Li and Ripley (2009). *Ol* olivine, *Cr-spl* Cr-rich spinel, *Opx* orthopyroxene, *Cpx* clinopyroxene, *Pl* Plagioclase, *Tmt* titanomagnetite

et al. 1990, 1994). This means that once magma reaches sulfide saturation, PGE are more compatible in sulfide liquid relative to Cu and Ni, which would lead a high Cu/Pd value in the residual magma (Barnes et al. 1993). The Cu/Pd values of the Baima rocks range from 1.9×10^6 to 6.1×10^4, and are of the same order of magnitudes as the sulfide-mineralized samples from the Limahe Cu-Ni deposit, which is considered to be related to second-stage sulfide segregation by Tao et al. (2008). However, the Baima Cu/Pd values are clearly higher than those of the PGE-undepleted Emeishan high-Ti basalts (Cu/Pd = 10^3–10^4) (Zhong et al. 2006; Qi et al. 2008; Qi and Zhou 2008; Song et al. 2009) (Fig. 8) and also are obviously higher than the Stella Pt–Pd deposit in South Africa and the Jinbaoshan Pt–Pd deposit in the central ELIP, which are considered to be formed from a single of sulfide segregation (Maier et al. 2003; Tao et al. 2007) (Fig. 8). Hence, the high Cu/Pd values imply that the parental magma of the Baima intrusion had already experienced sulfide segregation before entering the shallower magma chamber. However, three magnetite troctolites in the LZa have relatively higher Cu/Pd ($1.7 - 5.3 \times 10^4$) and similar or slightly higher PGE contents than the Emeishan high-Ti basalts (Figs. 8, 9). This suggests that some pulses of magma were not PGE-depleted when they intruded into the Baima intrusion.

Pd and Zr are highly incompatible in silicate minerals and hence concentrate in the residual magma during fractionation process. However, as Zr is a lithophile element and Pd is highly chalcophile, segregation of sulfide liquids will lead to an increase in the Pd/Zr in the fractionating solids, and a corresponding decrease in Pd/Zr of the residual melts (Lightfoot and Keays 2005). The PGE-depleted

samples in the Baima intrusion have much lower Pd/Zr (Pd/Zr < 0.1) than primitive mantle (Pd/Zr = 1.2), which may be explained by prior sulfide removal. In contrast, the three magnetite troctolites in the LZa which have relatively higher Cu/Pd values also have relatively high Pd/Zr (0.34–2.2), indicating that the parental magmas of these layers were relatively less PGE-depleted. The amount of sulfide segregated from the primary magma of the Baima intrusion can be estimated by the Rayleigh fractionation equation:

$$C_L = C_O * F^{(D-1)} \quad (1)$$

where C_L, the concentration of the element in the fractionated magma; C_O, concentration of an element in the initial magma; F, the fraction of melt remaining and D, the partition coefficient of the element. Assuming that the Pd content of the initial magma is 7.93 ppb, the data are estimated by Li et al. (2012), and the average palladium concentration of each zone as C_L (except three composition reversals at the lower zone). Using a partition coefficient of 3.4×10^4 for Pd between silicate and sulfide melt, calculations show that 0.007–0.012 % sulfides may have been removed from the initial magma at depth prior to emplacement of the Baima intrusion.

It has been recently suggested that the PGE-enriched layers in the Hongge and Xinjie intrusions are due to magmatic sulfide saturation triggered by external S addition and/or Fe–Ti oxide precipitation (Zhong et al. 2004, 2011b; Zhu et al. 2010; Bai et al. 2012a). Compared to the continental granite and sedimentary rocks, which has a broad range of $\delta^{34}S$ values, the narrow-scattered $\delta^{34}S$ values in the Baima intrusion probably indicate that external continental sulfides play a weak role (Table 3). This is consistent with previous Sr–Nd isotope data for Baima (Zhou et al. 2008), suggesting at most a weak, crustal contamination effect.

Selenium, which is much more abundant in mantle-derived magma than in crustal rocks has been used to constrain the formation of Cu-Ni sulfides and PGE deposits associated with mafic–ultramafic rocks (Eckstrand et al. 1989; Barnes et al. 2009). Primitive magmas typically have S/Se of 2,500–3,500 (Lorand et al. 2003), and high S/Se in such deposits has, in many studies, been taken as evidence that S has been contributed from the country rocks (Eckstrand and Hulbert 1987; Barnes et al. 2008, 2009). The lower S/Se values of the Baima intrusion further illustrate that crustal contamination (especially crustal S addition) did not play an important role in sulfide saturation (Fig. 7).

In S-undersaturated silicate melts, Ni and IPGE (Os, Ir, Ru) behave compatibly, preferring to concentrate in olivine, chromite and pyroxenes (Barnes et al. 1988, 2004; Capobianco and Drake 1990; Capobianco et al. 1994; Brenan and Rose 2002; Ely and Neal 2002). These elements exhibit high sulfide/silicate melt partition coefficient, and hence, once the magma reaches S saturation, they concentrate into the immiscible sulfide liquid. The sloping primitive mantle-normalized PGE patterns (Fig. 9) of the Baima rocks indicate that their parental magmas were initially S-undersaturated and experienced significant fractionation of silicate minerals before reaching sulfide saturation. Low Fo values in olivine (55–75) in the troctolites and gabbros indicate that the parental magmas of the Baima intrusion were highly evolved (Zhang et al. 2012). MELTS modeling indicates that the parental magmas were generated by ~61 % fractional crystallization of chromite, olivine and pyroxene from a high-Ti picritic magma at a

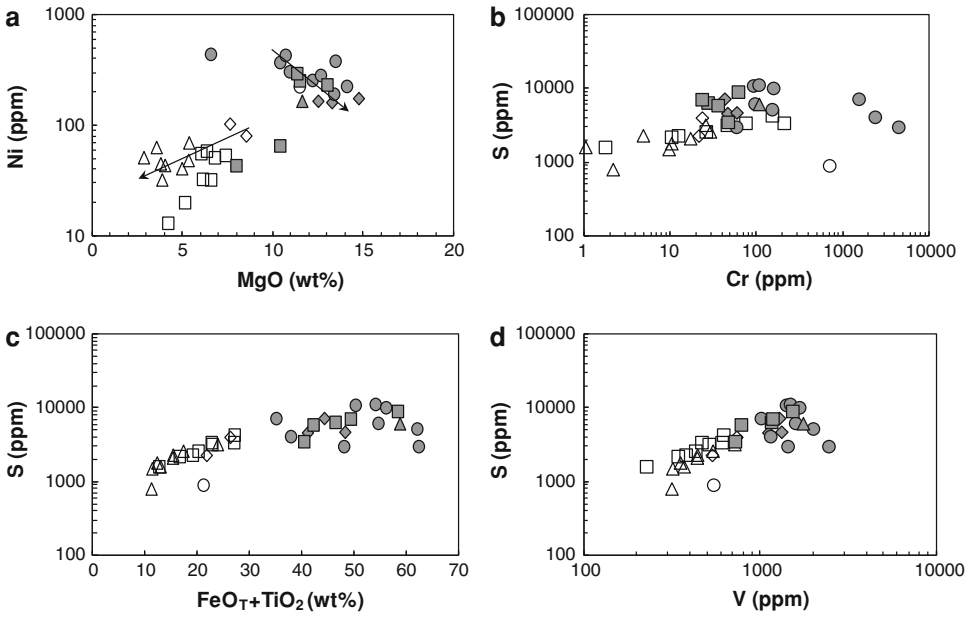

Fig. 11 Paired plots between ratios of Ni versus MgO (**a**), S versus Cr (**b**), S versus $FeO_T + TiO_2$ and V (**c**, **d**) in the Baima intrusion. *Troc* troctolite, *Gab* gabbro

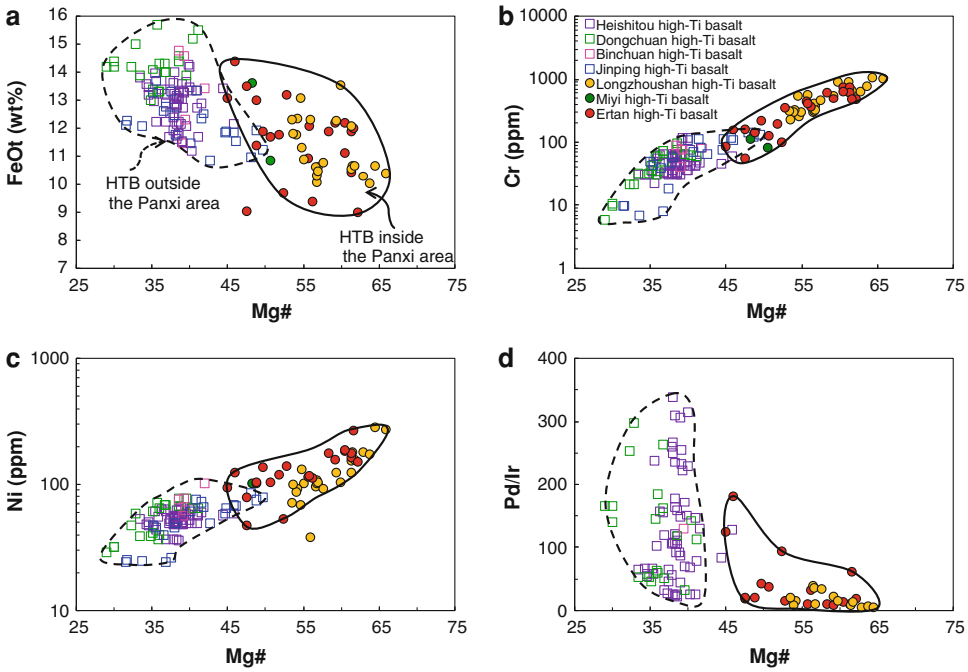

Fig. 12 Binary plots of major and trace elements with Mg number of the high-Ti basalts. The high-Ti basalts (HTB) inside the Panxi region (*circle*) are plot in the black line region, and the high-Ti basalts (HTB) outside the Panxi area (*square*) are plot in the dash line region. Data are from Xu et al. (2001), Zhong et al. (2006), Song et al. (2009), Wang et al. (2007), Qi et al. (2008) and Qi and Zhou (2008)

deep crustal levels (5 kbar) (Zhang et al. 2012). Using the equation of Li and Ripley (2009), and assuming 1,000 ppm as the initial S concentration of the primitive magma, calculations show that the magma could reach S saturation after ~ 59 % fractionation in the deep crust below the Baima intrusion (when the concentration of S in the silicate liquid reaches the S content at sulfide saturation (SCSS) value as shown in Fig. 10a). Hence, we suggest that S saturation and sulfide liquid immiscibility in the deep crust resulted from relatively high S concentration in the residual magma that was triggered by advanced fractional crystallization of silicate minerals.

Sulfide immiscibility in the Baima intrusion

The strong positive correlation between IPGE and PPGE (Fig. 5a, b) indicate that IPGE and PPGE are controlled by the same phase. Numerous experimental and empirical observations have shown that IPGE (Os, Ir, Ru) behave as compatible element in S-undersaturated mafic–ultramafic systems, preferentially concentrating in magnetite and chromite, whereas PPGE (Rh, Pt, Pd) behave incompatibly (Barnes and Picard 1993; Barnes et al. 2004; Brenan et al. 2012; Pagé et al. 2012 and references therein). Hence, IPGE abundances should correlate positively with the amount of magnetite or chromite, but the PPGE should not. In the Baima intrusion, V and Cr are dominantly concentrated in Fe–Ti oxides, especially in titanomagnetites. As shown in Fig. 6, the Ir shows less linear correlation with whole-rock V and Cr; however, Pd has a roughly positive correlation with whole-rock V and Cr. This illustrates that titanomagnetite is unlikely to be the main control on PGE distribution.

The partition coefficient of Ni between olivine and silicate melts ($D^{Ol/Sil}$) is 5.9–29, whereas the partition coefficient of Ni between sulfide and silicate melts ($D^{Sul/Sil}$ = 575–836) is considerably higher (Rollinson 1993; Gaetani and Grove 1997). Consequently, in a S-undersaturated system, Ni is compatible in olivine, but once the magma reaches S saturation, it will be strongly incorporated into sulfide. As shown in Fig. 11a, the roughly negative correlation between Ni and MgO in magnetite layers and slightly positive in barren troctolites and gabbros indicate that Ni abundances are not controlled by olivine but rather by immiscible sulfides in the magnetite layers and also suggest that sulfide melts may have segregated before olivine. Positive correlations between whole-rock Cr, $FeO_T + TiO_2$, V and S content further illustrate that precipitation of sulfides occurred simultaneously with early Fe–Ti oxides (Fig. 11b, c, d).

The three major variables controlling S solubility during fractional crystallization are: temperature, pressure and FeO content (Haughton et al., 1974; Wendlandt 1982; Lesher and Groves 1986; Mavrogenes and O'Neill 1999; Naldrett 2004). Wendlandt (1982) first found that S solubility decreased with increasing pressure and increased with increasing temperature. They predicted that a magma which is formerly S-saturated will become S-undersaturated during decompression and adiabatic ascent. Mavrogenes and O'Neill (1999) proved Wendlandt's work in a duplicated system and suggested that at low pressure, sulfide saturation should occur after substantial closed

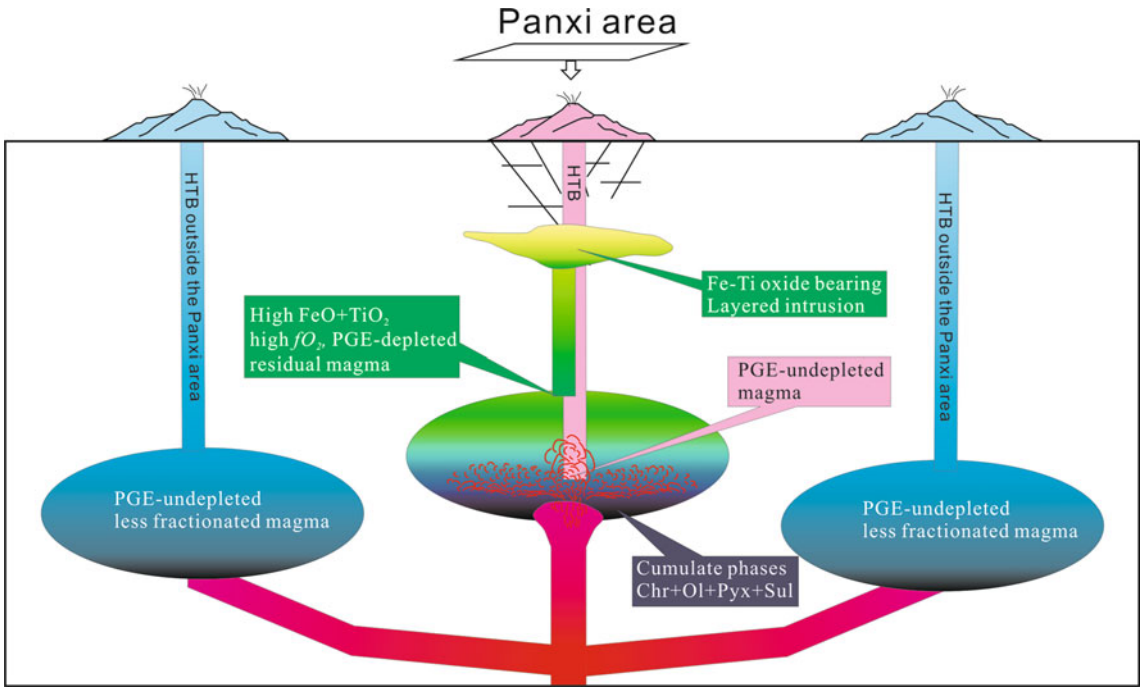

Fig. 13 A petrogenetic model showing the formation of the Baima intrusion and two types of high-Ti basalts in the ELIP. *Chr* chromite, *Ol* olivine, *Pyx* pyroxene, *Sul* sulfide

system crystallization (e.g., 60 % crystallization of olivine for a primitive picritic melt) or after crustal S addition. Furthermore, Prendergast (2000) and Maier et al. (2003) suggested that changes in phase equilibrium, especially Fe-oxide mineral crystallization can trigger the magma reach to S saturation. The mantle-derived sulfur isotope and the low S/Se ratios indicate that crustal S played a minor effect during crystallization of the Baima intrusion. Calculations using the equation of Li and Ripley (2009) show that such S-undersaturated magma can reach a 'second-stage' S saturation in the early stages of the Baima magma differentiation, in response to loss of Fe^{2+} due to titanomagnetite precipitation (Fig. 10b).

Genetic relationship between layered intrusion and high-Ti basalts

Based on geochemical data, Xu et al. (2001) subdivided the Emeishan high-Ti basalts into three groups: HT1, HT2, HT3. The HT1 group lavas are characterized with the highest TiO_2 (3.7–4.7 wt %), Fe_2O_3 (14.9–16.4 wt %) but the lowest $Mg^{\#}$ (0.32–0.42) content. They were sampled from Binchuan and Dongchuan area (Fig. 1). The HT2 lavas show moderate TiO_2 (2.5–3.9 wt %), Fe_2O_3 (12.7–16.4 wt %) and $Mg^{\#}$ (0.39–0.52) content. The HT3 lavas have the lowest TiO_2 (2.4–2.8 wt %), Fe_2O_3 (11.6–12.4 wt %) but the highest $Mg^{\#}$ (0.51–0.61) content. However, it is difficult to distinguish the HT2 and HT3 lavas in the field, because they were both sampled from Miyi and Ertan in the Panxi area (Fig. 2). Recent study found that the Emeishan high-Ti basalts have two distinct compositional features: the high-Ti basalts distributed outside the Panxi area and the high-Ti basalts from within the Panxi area (Bai et al. 2012b). The basalts located outside the Pan-Xi area have similar or slightly higher FeO_T (~13–16 wt %) contents and much lower MgO (~4–6 wt %) contents. In contrast, the basalts near the mafic–ultramafic intrusions in the Pan-Xi area have much lower FeO_T (9–14 wt %) contents and much higher MgO (5–10 wt %) contents than the basalts outside this area. They suggested that the former group (the high-Ti basalt outside the Panxi area) have not undergone abundant Fe–Ti oxide crystallization before their eruption; however, the latter may have undergone removal of Fe–Ti oxides in a deep magma chamber.

Unlike the Bushveld complexes and the Windimurra complex, in which economic Fe–Ti oxide layers commonly occur in the upper section of these layered intrusions (Wager and Brown 1968; Eales and Cawthorn 1996; Mathison and Ahmat 1996), thick Fe–Ti oxide layers in the Panxi area are usually present in the lower or middle parts of the layered intrusions and some of these host PGE-bearing layers (e.g. Hongge and Xinjie intrusions) (Pang et al. 2008, 2010; Zhong et al. 2002, 2004, 2005, 2011b, Bai et al. 2012a, b). This means that sulfide segregation may have occurred relatively earlier than, or simultaneously with, Fe–Ti oxide precipitation. If the high-Ti basalts inside the Panxi area were the evolved end-member

of the layered intrusions as suggested by Bai et al. (2012b), they should be depleted in PGE. Thus, this model contradicts the observed S-undersaturation feature shown by both groups of the high-Ti basalts (Zhong et al. 2006; Qi et al. 2008; Qi and Zhou 2008; Song et al. 2009; Wang et al. 2011).

As described above, the Baima intrusion was engulfed by later syenitic intrusions and dykes (PXGU 1984). However, direct contacts or intrusive relationships between the Hongge and Xinjie intrusions and the Emeishan high-Ti basalts indicate that the high-Ti basalts cannot be the evolved end-member liquid that formed these layered intrusions. As shown in Fig. 9, primitive mantle-normalized PGE patterns for the Baima intrusion display similar trends to high-Ti basalts from inside the Panxi area. Both show slight PPGE depletion relatively to high-Ti basalts outside the Panxi area. Furthermore, three PGE-enriched layers in the Baima intrusion also show similar primitive mantle-normalized PGE patterns to those of the high-Ti basalts inside the Panxi area. These data imply that the Baima intrusion and the high-Ti basalts inside the Panxi area were originally comagmatic and followed similar differentiation trends. The parental magma of the Baima intrusion may have experienced sulfide segregation before it rose to shallow crustal levels, whereas the parental magmas of high-Ti basalts inside the Panxi area and the three PGE-enriched layers in the Baima intrusion are more primitive and were erupted or intruded before their primary magma reached S saturation (Fig. 13).

Compared with the high-Ti basalts inside the Panxi area, the high-Ti basalts outside the Panxi area appear to be more evolved, with lower Mg#, Cr, Ni content and higher Pd/Ir values (Fig. 12). This illustrates that high-Ti basalts from outside the Panxi area may have experienced extensive fractional crystallization before eruption (Fig. 13). Further fractional crystallization process led these lavas to be depleted more in IPGE relative to PPGE (Fig. 9).

Conclusions

(1) The magma of the Baima layered intrusion experienced two stages of sulfide segregation. Extensive silicate fractional crystallization ($\sim$ 60 %) is the key factor controlling the first stage of sulfide segregation at deeper level, whereas early magnetite precipitation was important in triggering sulfide segregation in the shallower Baima chamber.

(2) The Baima intrusion and the Emeishan high-Ti basalts are originally broadly comagmatic, and followed similar differentiation trends; however, the parental magma of the Baima intrusion experienced sulfide segregation before intruding into a shallow magma chamber, whereas the parental magma of high-Ti basalts within the Panxi area and three recharge layers in the Baima intrusion were erupted or intruded before their primary magma reached to the S saturation.

(3) More evolved characteristics in the Emeishan high-Ti basalts from outside the Panxi area illustrate that these high-Ti basalts may have experienced more extensive fractional crystallization before erupting. Further fractional crystallization process led these lavas show more PGE fractionated feature.

(4) Deep-seated S saturation of the primary magma resulted in the Baima intrusion hosting only a giant Fe–Ti–V oxide deposit in the lower part of the intrusion, without economic PGE mineralization.

Acknowledgments Dr. Liang Qi, Dr. Shenghong Yang and Xiaowen Huang are gratefully acknowledged for PGE analysis. We appreciated Tony J. Crawford for improving the manuscript. We also thank Mike Lesher and an anonymous reviewer for their comments and golden suggestions. This work was funded by the National Basic Research Program of China (2012CB416804) and research fund of State Key Laboratory of Ore Deposit Geochemistry (SKLOG-ZY125-06) and NSFC research grants (40730420, 41172090) to Xie-Yan Song.

References

Andersen JCØ (2006) Postmagmatic sulphur loss in the Skaergaard intrusion: implications for the formation of the Platinova Reef. Lithos 92:198–221

Andersen JCØ, Rasmussen H, Nielsen TFD, Ronsbo JG (1998) The triple group and the Platinova gold and palladium reefs in the Skaergaard intrusion: stratigraphic and petrographic relations. Econ Geol 93:488–509

Bai ZJ, Zhong H, Li C, Zhu WG, Xu GW (2012a) Platinum-group elements in the oxide layers of the Hongge mafic–ultramafic intrusion, Emeishan Large Igneous Province, SW China. Ore Geol Rev 46:149–161

Bai ZJ, Zhong H, Naldrett AJ, Zhu WG, Xu GW (2012b) Whole-rock and mineral composition constraints on the genesis of the Giant Hongge Fe-Ti-V oxide deposit in the Emeishan large Igneous Province, Southwest China. Econ Geol 107:507–524

Barnes S-J, Picard C (1993) The behavior of platinum-group elements during partial melting, crystal fractionation, and sulphide segregation: an example from the Cape Smith Fold Belt, northern Quebec. Geochim Cosmochim Acta 57:79–87

Barnes S-J, Boyd R, Korneliussen A, Nilsson LP, Often M, Pedersen RB, Robins B (1988) The use of mantle normalization and metal ratios in discriminating between the effects of partial melting, crystal fractionation and sulphide segregation on platinum-group elements, gold, nickel and copper: examples from Norway. Geoplatinum 87:113–143

Barnes S-J, Couture JF, Sawyer EW, Bouchaib C (1993) Nickel-copper occurrences in the belleterre-angliers belt of the pontiac subprovince and the use of Cu-Pd ratios in interpreting platinum-group element distributions. Econ Geol 88:1402–1418

Barnes S-J, Maier W, Ashwal L (2004) Platinum-group element distribution in the main zone and upper zone of the Bushveld Complex, South Africa. Chem Geol 208:293–317

Barnes S-J, Prichard HM, Cox RA, Fisher PC, Godel B (2008) The location of the chalcophile and siderophile elements in platinum-group element ore deposits (a textural, microbeam and whole rock geochemical study): implications for the fort-nation of the deposits. Chem Geol 248:295–317

Barnes S-J, Savard D, Bedard LP, Maier WD (2009) Selenium and sulfur concentrations in the Bushveld Complex of South Africa and implications for formation of the platinum-group element deposits. Miner Depos 44:647–663

Brenan JM, Rose LA (2002) Experimental constraints on the wetting of chromite by sulfide liquid. Can Miner 40:1113–1126

Brenan JM, Finnigan CF, McDonough WF, Homolova V (2012) Experimental constraints on the partitioning of Ru, Rh, Ir, Pt and Pd between chromite and silicate melt: the importance of ferric iron. Chem Geol 302:16–32

Campbell IH, Naldrett AJ, Barnes SJ (1983) A model for the origin of the platinum-rich sulfide horizons in the Bushveld and Stillwater Complexes. J Petrol 24:133–165

Capobianco CJ, Drake MJ (1990) Partitioning of ruthenium, rhodium, and palladium between spinel and silicate melt and implications for platinum group element fractionation trends. Geochim Cosmochim Acta 54:869–874

Capobianco CJ, Hervig RL, Drake MJ (1994) Experiments on crystal/liquid partitioning of Ru, Rh and Pd for magnetite and hematite solid solutions crystallized from silicate melt. Chem Geol 113:23–43

Chen J, Yang X, Xiao L, He Q (2010) Coupling of basaltic magma evolution and lithospheric seismic structure in the Emeishan Large Igneous Province: MELTS modeling constraints. Lithos 119:61–74

Chung SL, Jahn B (1995) Plume-lithosphere interaction in generation of the Emeishan flood basalts at the Permian-Triassic boundary. Geology 23:889

Eales HV, Cawthorn RG (1996) The Bushveld Complex. In: Cawthorn (ed) Layered intrusion. Developments in petrology 15, Elsevier, Amsterdam, pp 181–229

Eckstrand OR, Hulbert LJ (1987) Selenium and the source of sulphur in magmatic nickel and platinum deposits: Geol. Assoc. Canada-Mineralog. Assoc. Canada Program with Abstracts 12, 40

Eckstrand OR, Grinenko LN, Krouse HR, Paktunc AD, Schwann PL, Scoates RF (1989) Preliminary data on sulphur isotopes and Se/S ratios, and the source of sulphur in magmatic sulphur in magmatic sulphides from the Fox River Sill, Molson Dykes and Thompson nickel deposits, northern Manitoba. In: Current Research, Part C. Geol Survey Can 89–1C pp 235–242

Ely JC, Neal CR (2002) Method of data reduction and uncertainty estimation for platinum-group element data using inductively coupled plasma-mass spectrometry. Geostand Geoanal Res 26:31–39

Gaetani GA, Grove TL (1997) Partitioning of moderately siderophile elements among olivine, silicate melt, and sulfide melt: constraints on core formation in the Earth and Mars. Geochim Cosmochim Acta 61:1829–1846

Govindaraju K (1994) 1994 complication of working values and sample description for 383 geostandards. Geostand Geoanal Res 18:158

Haughton DR, Roeder PL, Skinner BJ (1974) Solubility of sulfur in mafic magmas. Econ Geol 69:451–467

He B, Xu YG, Chung SL, Xiao L, Wang Y (2003) Sedimentary evidence for a rapid, kilometer-scale crustal doming prior to the eruption of the Emeishan flood basalts. Earth Planet Sci Lett 213:391–405

He B, Xu YG, Huang XL, Luo ZY, Shi YR, Yang QJ, Yu SY (2007) Age and duration of the Emeishan flood volcanism, SW China: geochemistry and SHRIMP zircon U-Pb dating of silicic ignimbrites, post-volcanic Xuanwei Formation and clay tuff at the Chaotian section. Earth Planet Sci Lett 255:306–323

Kamenetsky VS, Chung SL, Kamenetsky MB, Kuzmin DV (2012) Picrites from the Emeishan Large Igneous Province, SW China: a compositional continuum in primitive magmas and their respective mantle sources. J Petrol 53:2095–2113

Lesher CM, Groves DI (1986) Controls on the formation of komatiite-associated nickel-copper sulfide deposits. In: Friedrich GH, Genkin A, Naldrett AJ, Ridge JD, Sillitoe RH, Vokes FM (eds) Geology and metallogeny of copper deposits. Springer, Berlin, pp 43–62

Li C, Ripley EM (2009) Sulfur contents at sulfide-liquid or anhydrite saturation in silicate melts: empirical equations and example applications. Econ Geol 104:405–412

Li C, Tao Y, Qi L, Ripley EM (2012) Controls on PGE fractionation in the Emeishan picrites and basalts: constraints from integrated lithophile-siderophile elements and Sr-Nd isotopes. Geochim Cosmochim Acta 90:12–32

Lightfoot PC, Keays RR (2005) Siderophile and chalcophile metal variations in flood basalts from the Siberian trap, Noril'sk region: implications for the origin of the Ni-Cu-PGE sulfide ores. Econ Geol 100:439–462

Lorand JP, Alard O, Luguet A, Keays RR (2003) Sulfur and selenium systematics of the subcontinental lithospheric mantle: inferences from the Massif Central xenolith suite (France). Geochim Cosmochim Acta 67:4137–4151

Maier WD, Barnes S-J, Gartz V, Andrews G (2003) Pt-Pd reefs in magnetitites of the Stella layered intrusion, South Africa: a world of new exploration opportunities for platinum group elements. Geology 31:885–888

Mathison CI, Ahmat AL (1996) The Windimurra Complex, Western Australia. Dev Petrol 15:485–510

Mavrogenes JA, O'Neill HSC (1999) The relative effects of pressure, temperature and oxygen fugacity on the solubility of sulfide in mafic magmas. Geochim Cosmochim Acta 63:1173–1180

McCallum I (1996) The stillwater complex. In: Cawthorn RG (ed) Layered intrusion. Developments in petrology 15. Elsevier, Amsterdam, pp 441–483

Meisel T, Moser J (2004) Reference materials for geochemical PGE analysis: new analytical data for Ru, Rh, Pd, Os, Ir, Pt and Re by isotope dilution ICP-MS in 11 geological reference materials. Chem Geol 208:319–338

Naldrett AJ (2004) Magmatic sulfide deposits: Geology, geochemistry and exploration. Springer

Pagé P, Barnes S-J, Bédard JH, Zientek ML (2012) In situ determination of Os, Ir, and Ru in chromites formed from komatiite, tholeiite and boninite magmas: implications for chromite control of Os, Ir and Ru during partial melting and crystal fractionation. Chem Geol 302–303:3–15

Pang KN, Zhou MF, Lindsley D, Zhao D, Malpas J (2008) Origin of Fe-Ti oxide ores in mafic intrusions: evidence from the Panzhihua intrusion, SW China. J Petrol 49:295–313

Pang KN, Zhou MF, Qi L, Shellnutt G, Wang CY, Zhao DG (2010) Flood basalt-related Fe-Ti oxide deposits in the Emeishan large igneous province, SW China. Lithos 119:123–136

Panxi Geological Unit (1984) Mineralization and exploration forecasting of V-Ti magnetite deposits in the Panzhihua-Xichang region. (in Chinese)

Peach CL, Mathez EA, Keays RR (1990) Sulfide melt - silicate melt distribution coefficients for noble metals and other chalcophile elements as deduced from MORB: implications for partial melting. Geochim Cosmochim Acta 54:3379–3389

Peach CL, Mathez EA, Keays RR, Reeves SJ (1994) Experimentally determined sulfide melt-silicate melt partition-coefficients for iridium and palladium. Chem Geol 117:361–377

Prendergast M (2000) Layering and precious metals mineralization in the; Rincón del Tigre Complex, Eastern Bolivia. Econ Geol 95:113–130

Qi L, Zhou MF (2008) Platinum-group elemental and Sr-Nd-Os isotopic geochemistry of Permian Emeishan flood basalts in Guizhou Province, SW China. Chem Geol 248:83–103

Qi L, Hu J, Gregoire DC (2000) Determination of trace elements in granites by inductively coupled plasma mass spectrometry. Talanta 51:507–513

Qi L, Zhou MF, Wang CY (2004) Determination of low concentrations of platinum group elements in geological samples by ID-ICP-MS. J Anal Atom Spectrom 19:1335–1339

Qi L, Zhou MF, Wang CY, Sun M (2007) Evaluation of a technique for determining Re and PGEs in geological samples by ICP-MS coupled with a modified Carius tube digestion. Geochem J 41:407–414

Qi L, Wang CY, Zhou MF (2008) Controls on the PGE distribution of Permian Emeishan alkaline and peralkaline volcanic rocks in Longzhoushan, Sichuan Province, SW China. Lithos 106:222–236

Rollinson HR (1993) Using geochemical data: evaluation, presentation, interpretation. Longman, Singapore, pp 90–91

Sá JHS, Barnes S-J, Prichard HM, Fisher PC (2005) The distribution of base metals and platinum-group elements in magnetitite and its host rocks in the Rio Jacare Intrusion, Northeastern Brazil. Econ Geol 100:333–348

Shellnutt JG, Zhou MF, Zellmer GF (2009) The role of Fe-Ti oxide crystallization in the formation of A-type granitoids with implications for the Daly gap: an example from the Permian Baima igneous complex, SW China. Chem Geol 259:204–217

Song XY, Zhou MF, Hou ZQ, Cao ZM, Wang YL, Li YG (2001) Geochemical constraints on the mantle source of the upper permian Emeishan continental flood basalts, southwestern China. Int Geol Rev 43:213–225

Song XY, Zhou MF, Cao ZM, Robinson PT (2004) Late permian rifting of the South China Craton caused by the Emeishan mantle plume? J Geol Soc 161:773–781

Song XY, Zhang CJ, Hu RZ, Zhong H, Zhou MF, Ma RZ, Li YG (2005) Genetic links of magmatic deposits in the Emeishan large igneous province with dynamics of mantle plume. J Mineral Petrol 25:35–44 (in Chinese)

Song XY, Qi HW, Robinson PT, Zhou MF, Cao ZM, Chen LM (2008a) Melting of the subcontinental lithospheric mantle by the Emeishan mantle plume; evidence from the basal alkaline basalts in Dongchuan, Yunnan, Southwestern China. Lithos 100:93–111

Song XY, Zhou MF, Tao Y, Xiao JF (2008b) Controls on the metal compositions of magmatic sulfide deposits in the Emeishan large igneous province, SW China. Chem Geol 253:38–49

Song XY, Keays RR, Xiao L, Qi HW, Ihlenfeld C (2009) Platinum-group element geochemistry of the continental flood basalts in the central Emeisihan Large Igneous Province, SW China. Chem Geol 262:246–261

Tao Y, Li CS, Hu RZ, Ripley E, Du AD, Zhong H (2007) Petrogenesis of the Pt-Pd mineralized Jinbaoshan ultramafic intrusion in the Permian Emeishan Large Igneous Province, SW China. Contrib Mineral Petrol 153:321–337

Tao Y, Li C, Song XY, Ripley EM (2008) Mineralogical, petrological, and geochemical studies of the Limahe mafic-ultramatic intrusion and associated Ni-Cu sulfide ores, SW China. Mineral Depos 43:849–872

Taylor SR, McLennan SM (1985) The continental crust: its composition and evolution. Blackwell, Oxford, p 312

Wager LR, Brown GM (1968) Layered igneous rocks. Edinburgh, London

Wang CY, Zhou MF, Qi L (2007) Permian flood basalts and mafic intrusions in the Jinping (SW China) Song Da (northern Vietnam) district: mantle sources, crustal contamination and sulfide segregation. Chem Geol 243:317–343

Wang CY, Zhou MF, Qi L (2011) Chalcophile element geochemistry and petrogenesis of high-Ti and low-Ti magmas in the Permian Emeishan large igneous province, SW China. Contrib Mineral Petrol 161:237–254

Wendlandt RF (1982) Sulfide saturation of basalt and andesite melts at high pressures and temperatures. Am Min 67:877–885

Wilson A, Chunnett G (2006) Trace element and platinum group element distributions and the genesis of the Merensky Reef, western Bushveld Complex, South Africa. J Petrol 47:2369–2403

Xiao L, Xu YG, Mei HJ, Zheng YF, He B, Pirajno F (2004) Distinct mantle sources of low-Ti and high-Ti basalts from the western Emeishan large igneous province, SW China: implications for plume-lithosphere interaction. Earth Planet Sci Lett 228:525–546

Xu YG, Chung SL, Jahn BM, Wu GY (2001) Petrologic and geochemical constraints on the petrogenesis of Permian-Triassic Emeishan flood basalts in southwestern China. Lithos 58:145–168

Zhang XQ, Song XY, Chen LM, Xie W, Yu SY, Zheng WQ, Deng YF, Zhang JF, Gui SG (2012) Fractional crystallization and the formation of thick Fe–Ti–V oxide layers in the Baima layered intrusion, SW China. Ore Geol Rev 49:96–108

Zhong H, Zhu WG (2006) Geochronology of layered mafic intrusions from the Pan-Xi area in the Emeishan large igneous province, SW China. Miner Depos 41:599–606

Zhong H, Zhou XH, Zhou MF, Sun M, Liu BG (2002) Platinum-group element geochemistry of the Hongge Fe-V-Ti deposit in the Pan-Xi area, southwestern China. Miner Depos 37:226–239

Zhong H, Yao Y, Hu SF, Zhou XH, Liu BG, Sun M, Zhou MF, Viljoen MJ (2003) Trace-element and Sr-Nd isotopic geochemistry of the PGE-bearing Hongge layered intrusion, southwestern China. Int Geol Rev 45:371–382

Zhong H, Yao Y, Prevec SA, Wilson AH, Viljoen MJ, Viljoen RP, Liu BG, Luo YN (2004) Trace-element and Sr-Nd isotopic geochemistry of the PGE-bearing Xinjie layered intrusion in SW China. Chem Geol 203:237–252

Zhong H, Hu RZ, Wilson AH, Zhu WG (2005) Review of the Link Between the Hongge Layered Intrusion and Emeishan Flood Basalts, Southwest China. Int Geol Rev 47:971–985

Zhong H, Zhu WG, Qi L, Zhou MF, Song XY, Zhang Y (2006) Platinum-group element (PGE) geochemistry of the Emeishan basalts in the Pan-Xi area, SW China. Chin Sci Bull 51:845–854

Zhong H, Campbell IH, Zhu WG, Allen CM, Hu RZ, Xie LW, He DF (2011a) Timing and source constraints on the relationship between mafic and felsic intrusions in the Emeishan large igneous province. Geochim Cosmochim Acta 75:1374–1395

Zhong H, Qi L, Hu RZ, Zhou MF, Gou TZ, Zhu WG, Liu BG, Chu ZY (2011b) Rhenium-osmium isotope and platinum-group elements in the Xinjie layered intrusion, SW China: implications for source mantle composition, mantle evolution, PGE fractionation and mineralization. Geochim Cosmochim Acta 75:1621–1641

Zhou MF, Malpas J, Song XY, Robinson PT, Sun M, Kennedy AK, Lesher CM, Keays RR (2002) A temporal link between the Emeishan large igneous province (SW China) and the end-Guadalupian mass extinction. Earth Planet Sci Lett 196:113–122

Zhou MF, Robinson PT, Lesher CM, Keays RR, Zhang CJ, Malpas J (2005) Geochemistry, petrogenesis and metallogenesis of the Panzhihua gabbroic layered intrusion and associated Fe-Ti-V oxide deposits, Sichuan Province, SW China. J Petrol 46:2253–2280

Zhou MF, Arndt NT, Malpas J, Wang CY, Kennedy AK (2008) Two magma series and associated ore deposit types in the Permian Emeishan large igneous province, SW China. Lithos 103: 352–368

Zhu WG, Zhong H, Hu RZ, Liu BG, He DF, Song XY, Deng HL (2010) Platinum-group minerals and tellurides from the PGE-bearing Xinjie layered intrusion in the Emeishan Large Igneous Province, SW China. Miner and Petrol 98:167–180